lubricants

MDPI

Article

Simple Laser-Induced Hexagonal Boron Nitride Nanospheres for Enhanced Tribological Performance

Wei Li [1], Ting Luo [2,*], Changxu Zhu [2], Dalong Xu [2], Yifan Dong [2] and Bingqiang Cao [1,*]

[1] School of Material Science and Engineering, University of Jinan, Jinan 250022, China
[2] School of Mechanical and Automotive Engineering, Qilu University of Technology (Shandong Academy of Sciences), Jinan 250353, China
* Correspondence: tingluo_mae@qlu.edu.cn (T.L.); mse_caobq@ujn.edu.cn (B.C.)

Abstract: Hexagonal boron nitride, as a layered material with a graphite-like structure, exhibits good mechanical, lubricating and oxidation resistance properties, and is thus expected to become one of the top choices for green lubricating oil additives. However, its poor dispersibility in oil and difficulties in preparing spherical particles when constructing hexagonal boron nitride limit its application. In this paper, spherical hexagonal boron nitride nanoparticles are constructed via a simple laser irradiation method. Under laser irradiation, raw irregular hexagonal boron nitride particles were reshaped into nanospheres via a laser-induced photothermal process and rapid cooling in a liquid-phase environment. Under the optimal concentration, the coefficient of friction and wear spot diameter decreased by 26.1% and 23.2%, and the surface roughness and wear volume decreased by 29.2% and 23.8%, respectively. The enhanced tribological performance is mainly due to the ball bearing, depositional absorption and repair effect of the spherical particles. This simple laser irradiation method provides a new method by which to prepare spherical hexagonal boron nitride lubricating oil additives.

Keywords: hexagonal boron nitride; laser irradiation; tribological performance; lubrication mechanism

check for updates

Citation: Li, W.; Luo, T.; Zhu, C.; Xu, D.; Dong, Y.; Cao, B. Simple Laser-Induced Hexagonal Boron Nitride Nanospheres for Enhanced Tribological Performance. *Lubricants* **2023**, *11*, 199. https://doi.org/10.3390/lubricants11050199

Received: 28 March 2023
Revised: 26 April 2023
Accepted: 28 April 2023
Published: 29 April 2023

1. Introduction

Friction is a common phenomenon in nature, and beneficial friction can generate electric charges and provide triboelectricity, thus providing energy concentration [1]. However, most friction is harmful, and usually leads to a large amount of energy waste in the machining process, shortens the life of the machine and even causes potential safety risks [2,3]. Applying lubricating oil is the most effective strategy used to reduce wear and improve the efficiency of the machine [4–8]. Lubricating oil is composed of a base oil and additives. Therefore, it is an effective way of improving the quality of lubricating oil in order to prepare new lubricating oil additives and continuously improve the anti-wear and anti-friction properties of additives.

Two-dimensional layered materials, such as graphene, molybdenum disulfide and calcium fluoride, exhibit excellent tribological properties because of their special physical and chemical properties [3,9–14]. Among them, hexagonal boron nitride (*h*-BN) is a layered material with a graphite-like structure. Due to good mechanical, lubricating and oxidation resistance, it is expected to become one of the top choices for green lubricating oil additives after reasonable development [15]. Over the past few decades, plenty of studies on *h*-BN as a lubricating additive have been reported [2,16–22]. Yang et al. [2] found that as a friction additive in mineral oil, the as-prepared lipophilic BN nanosheets can reduce the coefficient of friction (COF) by 20.2%. More importantly, the track of the wear scar becomes significantly shallower. Urbaniak et al. [19] studied the tribological properties of BN as an additive to PAO4 base oil. They found that adding the *h*-BN layered nanomaterial to the lubricating oil can be a good solution for obtaining a lubricating oil with a ~27%

greater galling load than the base oil. Ma et al. [20] reported the successful exfoliation of BN nanosheets by combining a hydrothermal treatment at 180 °C with sonication. The exfoliated h-BN nanosheets possessed excellent friction reduction and anti-wear capabilities. Zang et al. [21] prepared BN/Cu nanocomposites by the in situ reduction of a mixture of $CuSO_4$ and BN with dopamine. The data showed that the liquid paraffin containing BN/Cu nanocomposites exhibited 27.3% lower COF and 25.3% lower wear scar diameters than pure liquid paraffin. However, the poor dispersion of *h*-BN nanoparticles in mineral oils limits its use [23]. At present, the chemical modification method is the main method used to solve the dispersion problem of nanoparticles in mineral oil, which needs to use certain chemical reagents [24]. Therefore, the preparation of lipophilic *h*-BN nanoparticles remains an ongoing challenge.

According to the anti-wear and anti-friction mechanism, because of the rolling effect of molecular bearings of spherical particles and the rapid formation of friction lubrication films between the friction pairs, spherical particles have more excellent lubrication properties. At present, the lubrication properties of spherical particles have been studied, such as iron oxide [25], carbon spheres [26–28], titanium dioxide [29] and tungsten disulfide [30]. *h*-BN has a strong (002) plane-oriented growth and is easily forms irregular flake nanoparticles. The currently reported methods used to prepare *h*-BN spherical particles usually require high temperatures above 1800 °C, urea, boric acid, ammonia and other chemicals, and the control of sphericity is still challenging [31–35].

Herein, a simple method that utilizes one-step laser irradiation in liquid at ambient conditions to prepare spherical *h*-BN is presented The synthesis process, without the use of any chemicals, is green and pollution free. After laser irradiation, the *h*-BN particles change from nanoflakes to spherical-shaped. At the same time, the surface charge of the *h*-BN particles increases greatly under laser photothermal action, which improves the dispersion of the *h*-BN particles in the base oil. The laser-induced *h*-BN (L-*h*-BN) spherical particles can be stably dispersed in the lubricating oil without settling for 30 days, and show excellent tribological properties. Under the optimal concentration, the coefficient of friction and wear spot diameter decreased by 26.1% and 23.2%, and the surface roughness and wear volume decreased by 29.2% and 23.8%, respectively. This study shows a new method by which to prepare spherical *h*-BN and its application in lubrication engineering.

2. Experimental Section

2.1. Preparation of the Hexagonal Boron Nitride (h-BN) Spherical Nanoparticles

The *h*-BN spherical nanoparticles were prepared via laser irradiation in the liquid phase. The raw material of hexagonal boron nitride was purchased. Raw *h*-BN nanoflakes (99.9% purity, Macklin, Shanghai, China) are an irregular flake shape. The average particle size of *h*-BN nanoflakes is approximately 100 nm. Then, 30 mL of deionized water was poured into a glass beaker, and 50 mg of *h*-BN was added to obtain an evenly dispersed *h*-BN liquid. A coherent KrF excimer laser (CompexPro 205, 248 nm, 25 ns, 10 Hz) was used as the laser irradiation source. The spot area of the laser beam was 0.7 cm^2, and the energy fluence values were 460, 500, 540 and 580 mJ $pulse^{-1}$ cm^{-2}. The laser irradiation lasted for 30 min. In the process of laser irradiation, in order to ensure the uniformity of the irradiation effect, magnetic stirring was used to treat the *h*-BN solution. Pictures of the liquid phase laser irradiation equipment are shown in Figure S1 (Supplementary Materials). After laser irradiation, the samples were dried for further characterization.

2.2. Material Characterizations

The Raman scattering spectrum was recorded by a Raman spectrometer (LabRAM HR Evolution, HORIBA, Kyoto, Japan, 532 nm). An X-ray diffractometer (XRD, D8-Advance, Bruker, Billerica, MA, USA) was used to test the crystal structures of different samples. X-ray photoelectron spectroscopy (XPS, Thermo Fisher, Waltham, MA, USA, Al Kα X-ray sources) was used to characterize the binding energies of N and B in different samples. The morphology of different samples was observed via a transmission electron microscope

(TEM, JEM-2100Plus). A three-dimensional optical microscope (Contour Elite K, Bruker, Billerica, MA, USA) was used to obtain the topography of the diameter of the wear scars on the surface of the steel balls.

2.3. Evaluation of the Tribological Property

The tribological properties of the h-BN particles were tested via a four-ball friction and wear testing machine (MM-W1B, Jinan, China). Before the experiment, the lubricating oil was poured into the oil tank, and the four steel balls were fully soaked in the lubricating oil. In the friction process, the top steel ball rotates (load: F, speed: ω), and the bottom three steel balls are fixed, as shown in Figure S2 (Supplementary Materials). After the friction experiment, the top steel ball formed an annular wear spot, and the bottom three steel balls formed a circular wear spot. The tribology tests were carried out at room temperature, the speed was 1000 rpm, the load was 392 N, and the test time was 30 min. The steel ball had a diameter of 12.7 mm, a hardness of 62 HRC, and was made of GCr15 bearing steel. During the friction tests, the COF was recorded in real time by software. The friction tests were repeated three times for each concentration, and the average value of the three tests was taken as the final data.

The *h*-BN nanoparticles prepared under different energy fluence values (460, 500, 540, 580 mJ pulse^{-1} cm^{-2}) were added into the PAO6 base oil at 0.05 wt% concentration, and the lubrication properties of the base oil containing additive were tested under the same friction condition. When the laser irradiation energy was 540 mJ pulse^{-1} cm^{-2}, the lubrication performance of the *h*-BN nanoparticles was the best, as shown in Figure S3 (Supporting Information). Therefore, we took the L-*h*-BN spherical nanoparticles prepared using 540 mJ pulse^{-1} cm^{-2} as an example in order to conduct detailed material characterization and tribological testing. In order to obtain the optimal additive concentration, the tribological properties of the *h*-BN nanoflakes and L-*h*-BN spherical nanoparticles with different mass concentrations (0.05 wt%, 0.1 wt%, 0.15 wt% and 0.2 wt%) were tested, respectively.

After the friction tests, the surface of the friction pairs was cleaned with petroleum ether, and then cleaned with alcohol for three times. The three-dimensional contour of the wear surface was observed with a three-dimensional optical microscope. The Raman scattering spectra of the materials on the wear surface were then recorded. The surface morphology of the friction pair was observed via a scanning electron microscope (SEM, FEI Quanta 250 FEG).

3. Results and Discussion

3.1. Preparation and Characterization of the L-h-BN Spheres

After laser irradiation, the high energy input rapidly produced a dissociation compression effect in the solution [36]. In addition, an extreme non-equilibrium state of ultrahigh temperature and ultrahigh pressure was induced on the interface between the laser beam and materials [37,38], which lead to the successful preparation of the spherical L-*h*-BN nanoparticles. The growth process is shown in Figure 1. The transformation of the particle morphology from flakes to spheres was accomplished in one step. When a laser beam first hit the raw *h*-BN slice, the laser spot exerted an immediate effect on the material interface. Under such impact, large slices of *h*-BN exploded into smaller pieces. Continuous pulsed laser irradiation caused heating and led to the surface melting of *h*-BN particles (process I in Figure 1). The raw *h*-BN particles were reshaped into nanospheres via a laser-induced photothermal process and rapid cooling in a liquid-phase environment [39] (Process II in Figure 1).

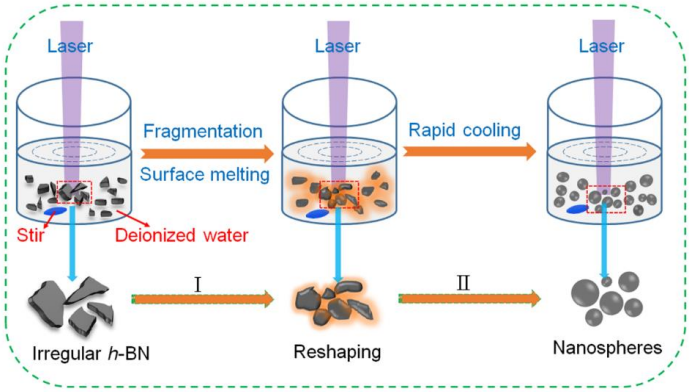

Figure 1. Schematic of the growth process of the spherical L-*h*-BN nanoparticles via a one-step laser irradiation method in ordinary water.

The morphology of the raw *h*-BN nanoflakes and L-*h*-BN spherical nanoparticles were characterized by TEM, as shown in Figure 2. The raw *h*-BN nanoflakes showed a flake structure and serious agglomeration phenomenon, as shown in Figure 2a. However, after simple laser irradiation, the *h*-BN changed from a flake structure to a spherical structure, and the particles became more loose. Then, the agglomeration phenomenon was suppressed. This is because under the action of laser irradiation, the absolute value of the Zeta potential on the surface of particles increases, and the repulsive force between particles increases, thus improving the dispersion of particles. Thus, compared with that of raw *h*-BN particles, the absolute value of the Zeta potential of the laser-induced *h*-BN nanospheres increased by 50%, as shown in Figure S4 (Supplementary Materials). High-power transmission electron microscopy (HTEM) images showed obvious lattice fringes with a lattice spacing of 0.33 nm. The L-*h*-BN spherical nanoparticles prepared in this study had a good size uniformity, ranging from 40 nm to 110 nm. The average particle size was around 80 nm (Figure S5 of Supplementary Materials). Using laser irradiation technology, when the laser irradiation energy was 540 mJ pulse^{-1} cm^{-2}, a spherical conversion rate of more than 95 was achieved.

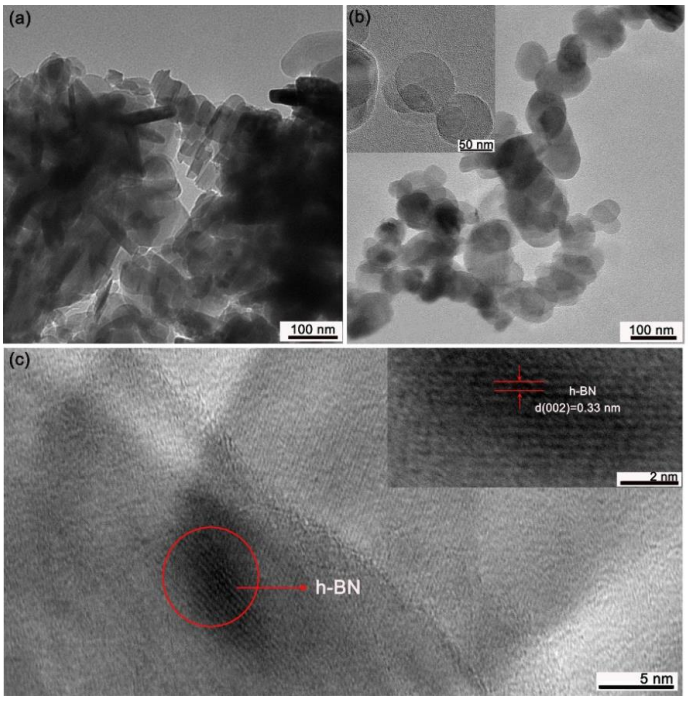

Figure 2. TEM images of (**a**) raw *h*-BN nanoflakes, (**b**) L-*h*-BN nanospheres grown via laser irradiation, and (**c**) HTEM images of L-*h*-BN nanospheres.

The phase of the raw *h*-BN nanoflakes and L-*h*-BN spherical nanoparticles was analyzed via XRD, as shown in Figure 3a. All XRD diffraction peaks could be assigned to the hexagonal phase of BN (JCPDS number: 34-0421 with P63/mmc space group). The *h*-BN crystal pattern did not change before and after laser irradiation. In addition, the diffraction peaks of h-BN were (002), (100), (101), (004), (110) and (112). After laser irradiation, the particle morphology changed from flake to spherical, resulting in a decrease in the intensity of the main reflection peak [40]. Figure 3b is the Raman spectra of the *h*-BN grown using different laser energy fluence values. The sharp Raman peak at 1366 cm^{-1} is mainly due to the high-frequency characteristic peak of h-BN. After laser treatment, the spherification of the *h*-BN particles resulted in a slight blue shift in the high-frequency Raman characteristic peaks [41].

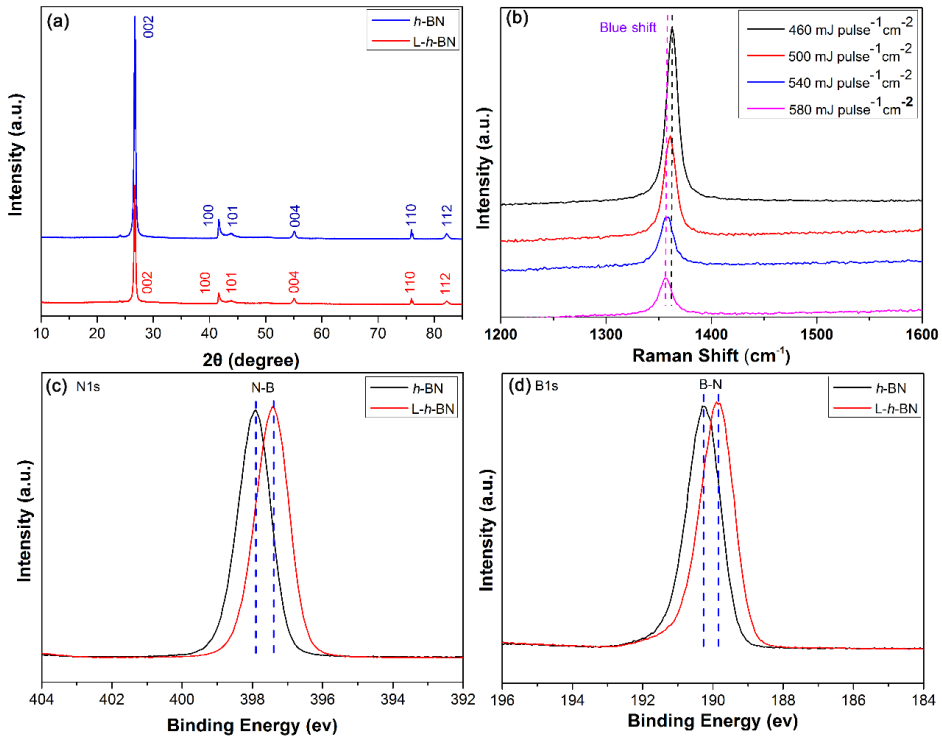

Figure 3. (**a**) XRD spectra of raw *h*-BN nanoflakes and L-*h*-BN nanospheres, and (**b**) Raman spectra of *h*-BN grown using different laser energy fluence values. XPS spectra of (**c**) N1s core-level and (**d**) B1s core-level for raw *h*-BN nanoflakes and L-*h*-BN nanospheres.

In order to analyze the changes in binding energy on the *h*-BN surface before and after laser irradiation, the XPS survey spectrum and core-level spectra of the aw *h*-BN nanoflakes and L-*h*-BN spherical nanoparticles were tested, as shown in Figures 3c,d and S6 (Supplementary Materials). The four distinct peaks observed in the XPS survey curve corresponded to B1s, N1s, O1s and C1s. Here, the existence of the O1s element may be due to the environmental existence of oxygen. All XPS survey curves show that mainly B and N were present in all the samples, which is in accordance with the XRD results. On the other hand, the C1s peak in the survey curve at 284.7 eV was possibly due to the carbon impurity and the environmental existence of carbon [42,43]. The core-level N1s and B1s spectra are displayed in Figure 3c,d, respectively. The presence of these peaks indicates the presence of B-N bonds in the samples [44,45]. It is worth noting that the binding energy of the N1s and B1s was shifted to a certain extent after laser irradiation. For the raw *h*-BN nanoflakes, the location of the N1s peak was at 397.91 ev, and the location of the B1s peak was at 190.29 ev. Meanwhile, for the laser-induced *h*-BN nanospheres, the location of the N1s peak was at 397.43 ev, and the location of the B1s peak was at 189.85 ev. This result further confirmed that the particles changed from flakes to spheres after laser irradiation [46].

The stable dispersion of lubricating oil additive in base oil is a prerequisite for its application. Spherical L-*h*-BN nanoparticles and *h*-BN nanoflakes were added to PAO6 base oil at 0.1% wt% concentration to observe the dispersion of nanoparticles in the base oil. Oil samples containing *h*-BN nanoflakes began to precipitate significantly after 3 days of standing (Figure 4a). However, for the oil sample containing spherical L-*h*-BN nanoparticles, the nanoparticles could still be stably dispersed in the base oil with the extension of the static time. There was no observable precipitation even after 30 days, suggesting that the spherical L-*h*-BN nanoparticles achieved good monodispersion in the base oil (Figure 4a). In order to further verify the dispersion stability of the additive, the absorbance curves of the spherical L-*h*-BN nanoparticles and *h*-BN nanoflakes in PAO6 were measured via a UV–visible spectrophotometer (Figure 4b). The absorbance of the PAO6 containing *h*-BN nanoflakes decreased rapidly with time under the irradiation of a 430 nm light source. In contrast, the absorbance of the PAO6 containing spherical h-BN nanoparticles was very stable, which proves that spherical *h*-BN nanoparticles disperse well in the PAO6 base oil.

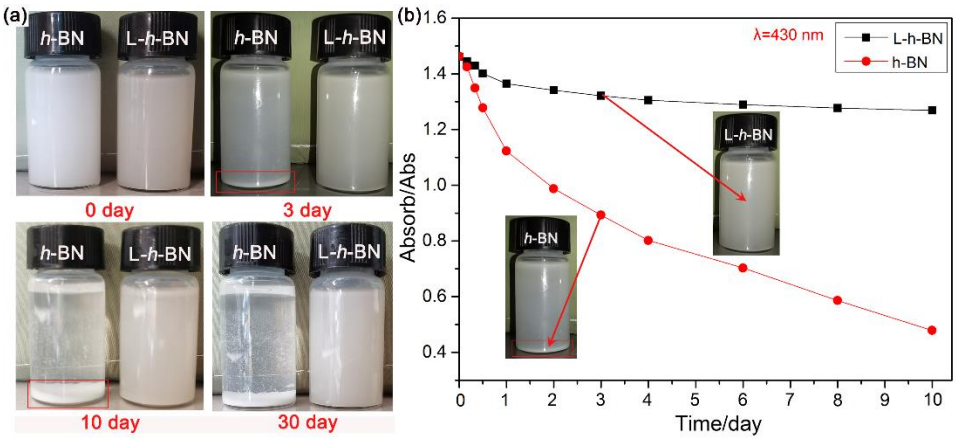

Figure 4. (**a**) Dispersion stability and (**b**) absorbency curves of *h*-BN nanoflakes and spherical L-*h*-BN nanoparticles in PAO6.

3.2. Friction Experiment

The tribological properties of the spherical L-*h*-BN nanoparticles were evaluated via a four-ball tribological test. The additive concentrations of the *h*-BN nanoflakes and spherical L-*h*-BN nanoparticles were 0.05 wt%, 0.1 wt%, 0.15 wt% and 0.2 wt%, respectively. The COF curve of the *h*-BN nanoflakes as a PAO6 additive at different concentrations is shown in Figure 5a. The COF of the pure PAO6 base oil was larger. However, after the addition of *h*-BN nanoflakes, the COF decreased gradually. For *h*-BN nanoflakes, when the concentration was less than 0.15 wt%, the COF decreased with increasing *h*-BN nanoflakes. The maximum reduction in the average COF was about 16.2% for PAO6 containing 0.1 wt% *h*-BN nanoflakes. The COF increased with a higher concentration of *h*-BN nanoflakes. The standard deviation of the COF curves of the oil samples with 0.1 wt% *h*-BN nanoflakes was 0.0008. However, the standard deviation of the COF curves of the oil samples with 0.1 wt% spherical L-*h*-BN was 0.00044. The COF curves of the oil samples with 0.1 wt% L-*h*-BN spherical nanoparticles were much smoother than the oil samples with 0.1 wt% *h*-BN nanoflakes, as shown in Figure 5a,c. When the PAO6 base oil contained 0.1 wt% spherical L-*h*-BN nanoparticles, the decrease of the COF reached the maximum 26.1% (Figure 5d), showing an excellent lubrication effect. This is because *h*-BN nanoflakes have poor dispersion in the base oil, and the aggregated *h*-BN nanoflakes easily scratched the surface of the friction pair, and the friction performance of the additive was not at its best [47]. The spherical L-h-BN nanoparticles were well dispersed in the base oil, successfully realizing the rolling friction between the friction pairs. In addition, during the friction process, the L-*h*-BN nanoparticles formed an excellent lubrication film on the surface of the friction pairs, thus reducing the COF [48].

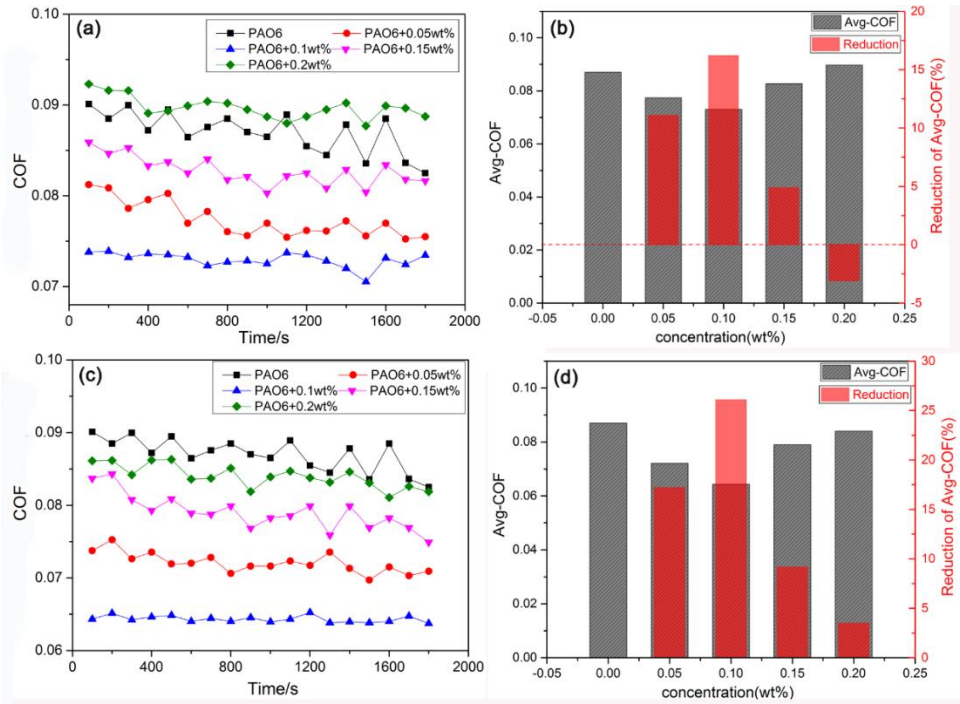

Figure 5. (**a**) COF curves of PAO6 base oil containing raw *h*-BN nanoflakes of different concentrations, (**b**) the corresponding average COF of raw *h*-BN nanoflakes with different concentrations and the COF reduction compared with pure PAO6, (**c**) COF curves of PAO6 base oil containing spherical L-*h*-BN nanoparticles of different concentrations, (**d**) the corresponding average COF of spherical L-*h*-BN nanoparticles with different concentrations and the COF reduction compared with pure PAO6.

Lubricating oil additives should not only have good anti-friction properties, but also have excellent anti-wear properties. After the friction experiment, the data of the wear scar diameter (WSD) on the fixing balls were studied (Figure 6). After the addition of L-*h*-BN spherical nanoparticles and *h*-BN nanoflakes, the WSD decreased, indicating that the additive had an anti-wear effect. However, when the concentration was greater than 0.1 wt%, the anti-wear effect began to weaken. This is because with the increase in the additive concentration, excess additives form caking, leading to serious wear [25]. When the concentration of spherical L-*h*-BN nanoparticles was 0.1 wt%, the WSD decreased the most, reaching 23.2%. At this time, the bearing pressure on the surface of the friction pair increased by 68.8% from 1.6 Gpa to 2.7 Gpa, and the load-bearing capacity was greatly improved. However, the dispersion effect of the *h*-BN nanoflakes was not as good as that of L-*h*-BN spherical nanoparticles. When the concentration of the *h*-BN nanoflakes was 0.2 wt%, the WSD increased compared with that of the pure base oil, which is the result of an agglomeration phenomenon. The excellent anti-wear performance is caused by two factors [41]. One is that the ball bearing effect leads to a low friction coefficient, thus reducing wear. On the other hand, after long friction, the L-*h*-BN spherical nanoparticles gradually peel off and change into lamellar structures during the process of friction and extrusion. As the friction process progresses, the lamellar structure adheres to the surface of the friction pair, reducing surface wear and repairing the friction pair.

After the friction experiment, the three-dimensional image of wear on the surface of the friction pair was obtained, as shown in Figure 7. When the L-*h*-BN was not added, the surface of the friction pair was seriously worn, and the furrows were deeper and wider (Figure 7a,b). A partially enlarged three-dimensional image (Figure 7c) shows severe fluctuations in the worn surface. After the addition of the L-*h*-BN spherical nanoparticles, the wear phenomenon was alleviated, and the fluctuation in the worn surface was greatly reduced, as shown in Figure 7d–f. Locally magnified three-dimensional images also show that the worn surface was relatively uniform and smooth. Finally, the surface roughness Ra

of the pure PAO6 friction pair was 3.012 µm, while that of the L-*h*-BN lubricating friction pair was 2.132 µm. The peak–valley difference in the friction pair surface decreased by 39.6%, from 7.809 µm to 4.717 µm. The wear volume decreased by 23.8%, from 0.0021 mm^3 to 0.0016 mm^3, indicating that the L-*h*-BN additive had better anti-wear effect.

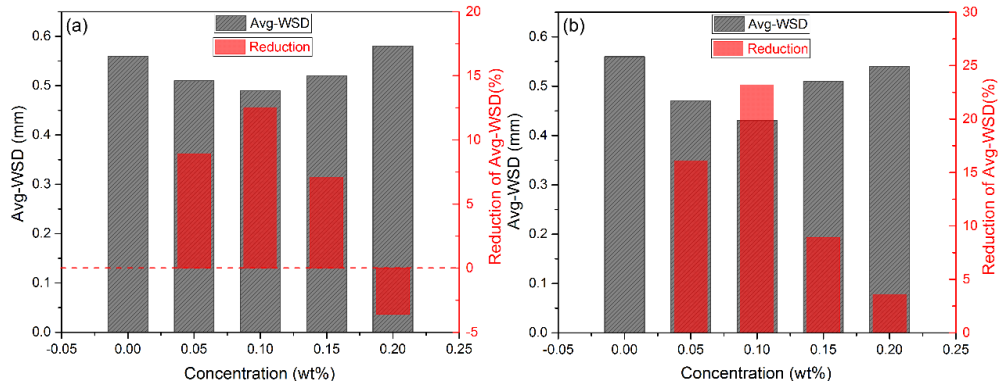

Figure 6. (**a**) Average WSD of each oil sample containing *h*-BN nanoflakes of different mass concentrations, and the corresponding WSD reduction is ascribed to the pure PAO6 base oil, (**b**) average WSD of each oil sample containing spherical L-*h*-BN nanoparticles of different mass concentrations, and the corresponding WSD reduction is ascribed to the pure PAO6 base oil.

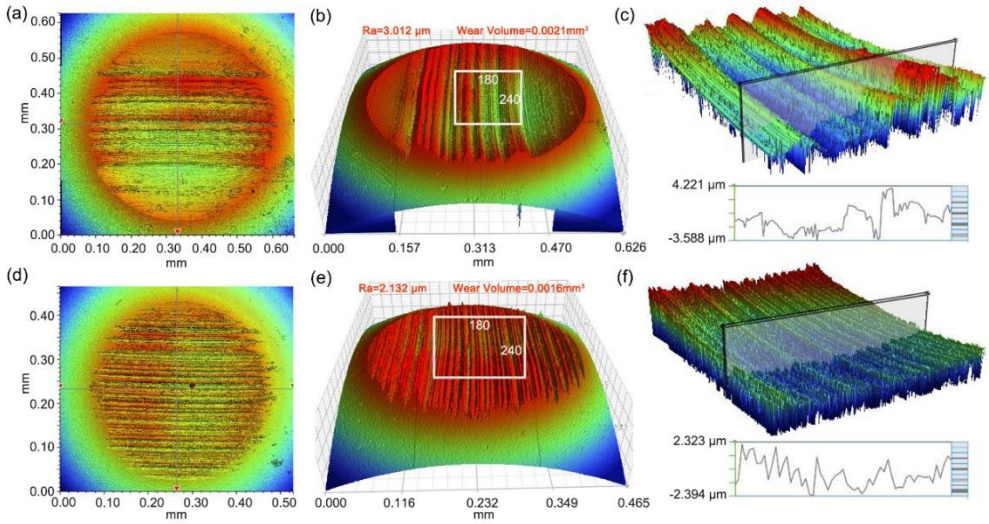

Figure 7. Three-dimensional optical images of wear surface after PAO6 friction test: (**a**) planar three-dimensional images, (**b**) solid three-dimensional images and (**c**) local enlarged three-dimensional images. Three-dimensional optical images of wear surface after PAO6 containing 0.1 wt% L-*h*-BN spherical nanoparticles friction test, (**d**) planar three-dimensional images, (**e**) solid three-dimensional images and (**f**) local enlarged three-dimensional images.

3.3. Mechanism Analysis

In order to explore the lubrication mechanism, a Raman spectrometer was used to analyze the worn surface, as shown in Figure 8. After the friction experiment with PAO6, the surface wear marks of the friction pair were found to be deep and wide (Figure 8a), consistent with the wear marks of the three-dimensional optical image. Raman analysis of the friction area showed a significant ferric oxide peak at ~667 cm^{-1}, indicating severe surface wear on the friction pair [49]. For the sample containing spherical L-*h*-BN, the worn surface was smooth and flat (Figure 8b). In addition, both the Raman spectra (Figure 8b) and Raman plane scanning mode (Figure 8c,d) of the worn surface showed an obvious L-*h*-BN signal, which indicates that the L-*h*-BN additive was uniformly deposited on the friction pairs. Therefore, the L-*h*-BN additive could effectively form a tribofilm and play a very important surface repair role, and exhibit a significant anti-wear effect [41].

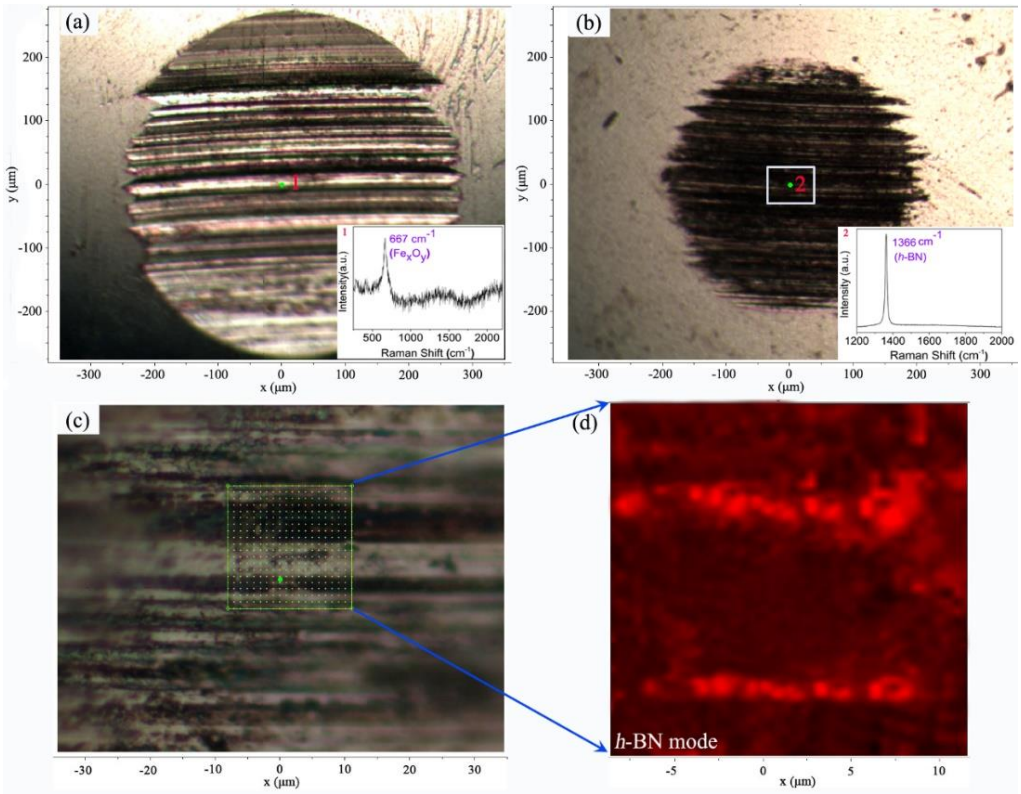

Figure 8. Optical images of the worn surface tested by (**a**) pure PAO6 and (**b**) PAO6 containing 0.1 wt% L-*h*-BN, (**c**) the enlarged image of the white box in the (**b**), and (**d**) Raman intensity mapping images of *h*-BN.

Figure 9a,b show the SEM images of the worn surface of the pure PAO6 and L-*h*-BN additive after friction tests, respectively. The images show that the worn surface lubricated with pure PAO6 after cleaning was uneven and had a large diameter. The worn surface lubricated with PAO6 containing L-*h*-BN additive was smooth and had a small diameter. Energy Dispersive Spectrometer (EDS) analysis was used to study the chemical composition of the worn surface, as shown in Figure 9c–e. The N element mapping image and the EDS spectrum showed that the worn surface of the L-*h*-BN additive contained the N element, which proved that the L-*h*-BN additive was successfully deposited on the surface of the friction pairs. After the friction test, the distribution of the N element showed a spherical shape, consistent with the appearance of the worn spot, indicating that *h*-BN was successfully deposited on the surface of the friction pair to form a tribofilm and that it played an important repairing role.

The lubrication mechanism of L-*h*-BN as oil additives is shown in Figure 10. L-*h*-BN nanospheres as additives can be well dispersed in the base oil. In the friction process, spherical nanoparticles can change sliding friction into rolling friction, thus reducing the COF, as shown in Figure 10b. In addition, some L-*h*-BN spherical additives can be stripped into lamellar layers during the extrusion of the friction pair. The lower shear force between the lamellar structures can also reduce the COF. As the friction process proceeds, the lamellar structure is adsorbed on the surface of the friction pair to form a tribofilm and repair the friction pair, thus reducing the surface wear and exerting the anti-wear effect (Figure 10d). In conclusion, under the combined action of the above two mechanisms, L-*h*-BN spherical nanoparticles as additives exhibit excellent anti-wear and anti-friction effects.

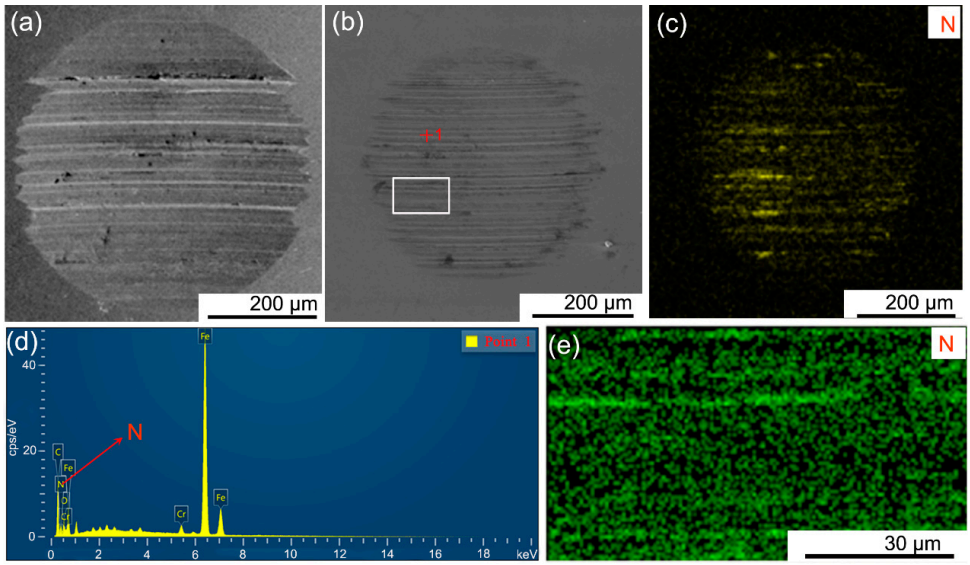

Figure 9. SEM images of worn surface lubricated with (**a**) pure PAO6 and (**b**) 0.1 wt% L-*h*-BN, (**c**) N element mapping image of friction pair surface lubricated with 0.1 wt% L-*h*-BN, (**d**) the EDS spectrum of point 1 in (**b**), (**e**) N element mapping image of the white box area in (**b**).

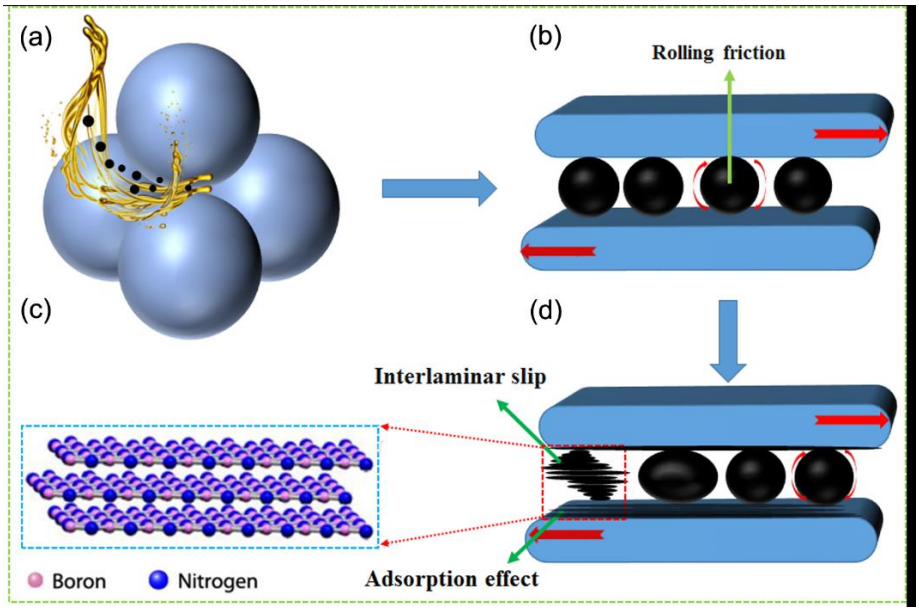

Figure 10. Lubrication mechanism of L-*h*-BN additive. (**a**) Diagram of four-ball friction, (**b**) rolling friction of nanospheres, (**c**) *h*-BN molecular structure, and (**d**) interlaminar slip of layered structure.

4. Conclusions

In the preceding sections, a simple laser irradiation method for preparing L-h-BN spherical nanoparticles is presented. The tribological properties of L-h-BN spherical nanoparticles as lubricating oil additives are also studied, and the lubrication mechanism is fully discussed.

1. As a lubricating additive, L-*h*-BN nanospheres can achieve good dispersion stability in PAO6 and maintain no precipitation for 30 days.

2. L-*h*-BN nanospheres show enhanced tribological performance. When the concentration of spherical L-*h*-BN nanoparticles is 0.1 wt%, the COF and WSD decrease by 26.1% and 23.2%, and the wear volume and surface roughness decrease by 23.8% and 29.2%, respectively.

3. Under the optimal addition concentration, the bearing pressure on the surface of the friction pair is increased by 68.8%, from 1.6 Gpa to 2.7 Gpa. The peak–valley difference in friction pair surface decreases by 39.6%, from 7.809 μm to 4.717 μm.

4. The anti-wear and anti-friction mechanism is caused by two main factors. First, the effect of the ball bearing leads to a low coefficient of friction. In addition, as the friction process progresses, some L-*h*-BN spherical nanoparticles gradually peel off and change into layered structures. The layered *h*-BN adheres to the worn surface to form a tribofilm, repairing the worn surface and reducing wear.

5. L-*h*-BN spherical nanoparticles have excellent anti-wear and anti-friction properties. This simple one-step laser irradiation method provides a new way to prepare spherical layered lubricating oil additives.

Supplementary Materials: The following supporting information can be downloaded at: https://www.mdpi.com/article/10.3390/lubricants11050199/s1, Figure S1: Pictures of Liquid phase laser irradiation equipment (a) side view, (b) front view; Figure S2: Diagram of four-ball friction and wear test model [50]; Figure S3: (a) COF curves of a base oil containing additives with different laser irradiation flux, (b) The corresponding average COF and the COF reduction compared with pure PAO6; Figure S4: Absolute value of zeta potential before and after laser irradiation; Figure S5: Particle size distribution of L-h-BN spherical nanoparticles; Figure S6: XPS survey spectrums of (a) raw h-BN nanoflakes and (b) L-h-BN spherical nanoparticles.

Author Contributions: Methodology, W.L. and C.Z.; software, D.X.; validation, W.L. and Y.D.; formal analysis, W.L.; investigation, C.Z.; resources, T.L.; data curation, W.L.; writing—original draft preparation, W.L.; writing—review and editing, T.L.; supervision, B.C.; project administration, T.L. and B.C.; funding acquisition, T.L. and B.C. All authors have read and agreed to the published version of the manuscript.

Funding: This work was supported by National Natural Science Foundation of China (51872161, Cao, B.), Shandong Province Natural Science Foundation (ZR2020QE160, Luo, T.) and Jinan Bureau of Science and Technology (2020GXRC020, Cao, B.).

Data Availability Statement: Not applicable.

Conflicts of Interest: The authors declare no conflict of interest.

References

1. Mariello, M. Recent Advances on Hybrid Piezo-Triboelectric Bio-Nanogenerators: Materials, Architectures and Circuitry. *Nanoenergy Adv.* **2022**, *2*, 64–109. [CrossRef]
2. Yang, W.; Geng, Z.; Li, Y.; Liu, X.; Tian, X.; Wang, S.; Wu, N.; Wang, Y.; Xu, R.; Yang, F.; et al. Facile synthesis of lipophilic alkylated boron nitride nanosheets as lubricating oil additive to greatly enhance the friction and heat-conducting properties. *Tribol. Int.* **2022**, *173*, 107655. [CrossRef]
3. Altavilla, C.; Sarno, M.; Ciambelli, P.; Senatore, A.; Petrone, V. New 'chimie douce' approach to the synthesis of hybrid nanosheets of MoS_2 on CNT and their anti-friction and anti-wear properties. *Nanotechnology* **2013**, *24*, 125601. [CrossRef] [PubMed]
4. Huang, Y.; Wang, J.; Yu, W.-J.; Yu, Y.; Li, R.-Y.; Gao, Q.; Ren, K.-F.; Ji, J. A Bioinspired Hydrogel-Elastomer Hybrid Surface for Enhanced Mechanical Properties and Lubrication. *ACS Appl. Mater. Interfaces* **2021**, *13*, 50461–50469. [CrossRef]
5. Guo, J.; Wu, P.; Zeng, C.; Wu, W.; Zhao, X.; Liu, G.; Zhou, F.; Liu, W. Fluoropolymer grafted Ti_3C_2Tx MXene as an efficient lubricant additive for fluorine-containing lubricating oil. *Tribol. Int.* **2022**, *170*, 107500. [CrossRef]
6. Sarno, M.; Scarpa, D.; Senatore, A.; Mustafa, W.A.A. rGO/GO Nanosheets in Tribology: From the State of the Art to the Future Prospective. *Lubricants* **2020**, *8*, 31. [CrossRef]
7. Gong, H.; Yu, C.; Zhang, L.; Xie, G.; Guo, D.; Luo, J. Intelligent lubricating materials: A review. *Compos. Part B Eng.* **2020**, *202*, 108450. [CrossRef]
8. Erdemir, A.; Ramirez, G.; Eryilmaz, O.L.; Narayanan, B.; Liao, Y.; Kamath, G.; Sankaranarayanan, S.K.R.S. Carbon-based tribofilms from lubricating oils. *Nature* **2016**, *536*, 67–71. [CrossRef]
9. Spear, J.C.; Ewers, B.W.; Batteas, J.D. 2D-nanomaterials for controlling friction and wear at interfaces. *Nano Today* **2015**, *10*, 301–314. [CrossRef]
10. Zhang, H. Ultrathin Two-Dimensional Nanomaterials. *ACS Nano* **2015**, *9*, 9451–9469. [CrossRef]
11. Bas, H.; Ozen, O.; Bes, I.G.M. Tribological properties of MoS_2 and CaF_2 particles as grease additives on the performance of block-on-ring surface contact. *Tribol. Int.* **2022**, *168*, 107433. [CrossRef]
12. Kinoshita, H. The use of graphene oxide as a lubricating additive. *Carbon* **2021**, *175*, 608–609. [CrossRef]

13. Wang, D.; Li, F.; Chen, X.; Li, H.; Chen, W.; Zhang, P. Effect of Two Graphene Coatings on the Friction and Wear of Sliding Electrical Contact Interface. *Lubricants* **2022**, *10*, 305. [CrossRef]
14. Sgroi, M.; Asti, M.; Gili, F.; Deorsola, F.; Bensaid, S.; Fino, D.; Kraft, G.; Garcia, I.; Dassenoy, F. Engine bench and road testing of an engine oil containing MoS_2 particles as nano-additive for friction reduction. *Tribol. Int.* **2017**, *105*, 317–325. [CrossRef]
15. Tian, Q.; Jia, X.H.; Zhang, Y.C.; Zhang, Y.P.; Yang, J.; Wang, S.Z.; Li, Y.; Shao, D.; Feng, L.; Song, H.J. In-situ growth of amorphous carbon on sucrose-assisted exfoliated boron nitride nanosheets: Exceptional water dispersibility and lubrication performance. *Tribol. Int.* **2022**, *173*, 107647. [CrossRef]
16. Zhu, Y.; Li, H.; Fei, J.; Li, C.; Ma, S.; Cai, X.; Li, B. Effect of modified nano boron nitride on tribological performance of resin-based friction material paired with copper dual disk. *Tribol. Int.* **2022**, *168*, 107429. [CrossRef]
17. Nadiège, N.M.; Manuella, V.; Henry, J.; Philippe, T. Moringa oil with graphite and hexagonal boron nitride particles as additives for lubrication. *Diam. Relat. Mater.* **2022**, *124*, 108930.
18. Kumari, S.; Chouhan, A.; Sharma, O.P.; Tawfik, S.A.; Spencer, M.J.S.; Bhargava, S.K.; Walia, S.; Ray, A.; Khatri, O.P. Alka-li-Assisted Hydrothermal Exfoliation and Surfactant-Driven Functionalization of h-BN Nanosheets for Lubrication Enhancement. *ACS Appl. Nano Mater.* **2021**, *4*, 9143–9154. [CrossRef]
19. Urbaniak, W.; Majewski, T.; Powązka, I.; Śmigielski, G.; Petelska, A.D. Study of Nano h-BN Impact on Lubricating Properties of Selected Oil Mixtures. *Materials* **2022**, *15*, 2052. [CrossRef]
20. Ma, Z.-S.; Ding, H.-L.; Liu, Z.; Cheng, Z.-L. Preparation and tribological properties of hydrothermally exfoliated ultrathin hexagonal boron nitride nanosheets (BNNSs) in mixed NaOH/KOH solution. *J. Alloys Compd.* **2019**, *784*, 807–815. [CrossRef]
21. Zang, C.; Yang, M.; Liu, E.; Qian, Q.; Zhao, J.; Zhen, J.; Zhang, R.; Jia, Z.; Han, W. Synthesis, characterization and tribological behaviors of hexagonal boron nitride/copper nanocomposites as lubricant additives. *Tribol. Int.* **2022**, *165*, 107312. [CrossRef]
22. Chen, Z.; He, X.; Xiao, C.; Kim, S.H. Effect of Humidity on Friction and Wear—A Critical Review. *Lubricants* **2018**, *6*, 74. [CrossRef]
23. Yu, C.P.; Zhang, Q.C.; Zhang, J.; Geng, R.J.; Tian, W.; Fan, X.D.; Yao, Y.G. One-step in situ ball milling synthesis of polymer-functionalized few-layered boron nitride and its application in high thermally conductive cellulose composites. *ACS Appl. Nano Mater.* **2018**, *1*, 4875–4883. [CrossRef]
24. Soudagar, M.E.M.; Nik-Ghazali, N.-N.; Kalam, M.; Badruddin, I.A.; Banapurmath, N.; Bin Ali, M.A.; Kamangar, S.; Cho, H.M.; Akram, N. An investigation on the influence of aluminium oxide nano-additive and honge oil methyl ester on engine performance, combustion and emission characteristics. *Renew. Energy* **2020**, *146*, 2291–2307. [CrossRef]
25. Song, X.Y.; Qiu, Z.W.; Yang, X.P.; Gong, H.B.; Zheng, S.H.; Cao, B.Q.; Wang, H.Q.; Möhwald, H.; Shchukin, D. Submicron-Lubricant Based on Crystallized Fe_3O_4 Spheres for Enhanced Tribology Performance. *Chem. Mater.* **2014**, *26*, 5113–5119. [CrossRef]
26. Xie, M.; Pan, B.; Liu, H.; Li, N.; Chen, Z.; Yan, J.; Fu, Z.; Guo, S.; Wang, H. One-step synthesis of carbon sphere@ 1 T-MoS_2 towards superior antiwear and lubricity. *Tribol. Int.* **2022**, *176*, 107927. [CrossRef]
27. Xu, J.X.; Chen, X.C.; Zmacher, P.G.; Rosenkranz, A.; Li, J.J.; Jin, J.; Zhang, C.H.; Luo, J.B. Tribochemical Behaviors of Onion-like Carbon Films as High-Performance Solid Lubricants with Variable Interfacial Nanostructures. *ACS. Appl. Mater. Inter.* **2019**, *11*, 25535–25546. [CrossRef]
28. Wu, L.; Zhang, Z.; Yang, M.; Yuan, J.; Li, P.; Guo, F.; Men, X. Mulberry-like carbon spheres decorated with UiO-66-NH_2 for enhancing the mechanical and tribological performances of UHMWPE composites. *Tribol. Int.* **2020**, *141*, 105916. [CrossRef]
29. Birleanu, C.; Pustan, M.; Cioaza, M.; Molea, A.; Popa, F.; Contiu, G. Effect of TiO_2 nanoparticles on the tribological properties of lubricating oil: An experimental investigation. *Sci. Rep.* **2022**, *12*, 5201. [CrossRef]
30. Hu, N.; Zhang, X.; Wang, X.; Wu, N.; Wang, S. Study on Tribological Properties and Mechanisms of Different Morphology WS_2 as Lubricant Additives. *Materials* **2020**, *13*, 1522. [CrossRef]
31. Liu, C.; Fu, K.; Wang, Z.; Cao, C.; Yang, J.; Zhai, Q.; Wang, B.; Zhou, Z.; Ji, J.; Li, M.; et al. Cavitating inside spherical boron nitride nanoparticles dependent on controllably follow-up treated atmospheres. *J. Nanopart. Res.* **2020**, *22*, 302. [CrossRef]
32. Zhang, N.; Liu, H.; Kan, H.; Wang, X.; Long, H.; Zhou, Y. The preparation of high-adsorption, spherical, hexagonal boron nitride by template method. *J. Alloys Compd.* **2014**, *613*, 74–79. [CrossRef]
33. Tang, C.; Bando, Y.; Huang, Y.; Zhi, C.; Golberg, D. Synthetic Routes and Formation Mechanisms of Spherical Boron Nitride Nanoparticles. *Adv. Funct. Mater.* **2008**, *18*, 3653–3661. [CrossRef]
34. Han, W.; Wang, J.; Liu, S.; Ge, C.; Cao, S.; Song, B.; Wang, J.; Zhang, X. Spectral properties of spherical boron nitride prepared using carbon spheres as template. *Ceram. Int.* **2017**, *43*, 3569–3575. [CrossRef]
35. Ren, L.; Zeng, X.; Sun, R.; Xu, J.-B.; Wong, C.-P. Spray-assisted assembled spherical boron nitride as fillers for polymers with enhanced thermally conductivity. *Chem. Eng. J.* **2019**, *370*, 166–175. [CrossRef]
36. Zhang, D.S.; Liu, J.; Liang, C.H. Perspective on how laser-ablated particles grow in liquids. *Sci. China Phys. Mech. Astron.* **2017**, *60*, 1–16. [CrossRef]
37. Adelmann, B.; Hellmann, R. A study of SiC decomposition under laser irradiation. *Appl. Phys. A-Mater.* **2017**, *123*, 454–459. [CrossRef]
38. Ding, Y.; Yang, L.; Hong, M. Enhancement of pulsed laser ablation assisted with continuous wave laser irradiation. *Sci. China Phys. Mech. Astron.* **2019**, *62*, 66–74. [CrossRef]
39. Hu, X.; Gong, H.; Wang, Y.; Chen, Q.; Zhang, J.; Zheng, S.; Yang, S.; Cao, B. Laser-induced reshaping of particles aiming at energy-saving applications. *J. Mater. Chem.* **2012**, *22*, 15947. [CrossRef]

40. Kumar, A.; Malik, G.; Sharma, S.; Chandra, R.; Mulik, R.S. Precursors controlled morphologies of nanocrystalline h-BN and its growth mechanism. *Ceram. Int.* **2021**, *47*, 30985–30992. [CrossRef]
41. Luo, T.; Wang, P.; Qiu, Z.; Yang, S.; Zeng, H.; Cao, B. Smooth and solid WS_2 submicrospheres grown by a new laser fragmentation and reshaping process with enhanced tribological properties. *Chem. Commun.* **2016**, *52*, 10147. [CrossRef] [PubMed]
42. Kumar, A.; Malik, G.; Chandra, R.; Mulik, R.S. Bluish emission of economical phosphor h-BN nanoparticle fabricated via mixing annealing route using non-toxic precursor. *J. Solid State Chem.* **2020**, *288*, 121430. [CrossRef]
43. Annamalai, M.; Gopinadhan, K.; Han, S.A.; Saha, S.; Park, H.J.; Cho, E.B.; Kumar, B.; Patra, A.; Kim, S.-W.; Venkatesan, T. Surface energy and wettability of van der Waals structures. *Nanoscale* **2016**, *8*, 5764–5770. [CrossRef] [PubMed]
44. Liu, Q.; Chen, C.; Du, M.; Wu, Y.; Ren, C.; Ding, K.; Song, M.; Huang, C. Porous Hexagonal Boron Nitride Sheets: Effect of Hydroxyl and Secondary Amino Groups on Photocatalytic Hydrogen Evolution. *ACS Appl. Nano Mater.* **2018**, *1*, 4566–4575. [CrossRef]
45. Chen, X.; Dmuchowski, C.M.; Park, C.; Fay, C.C.; Ke, C. Quantitative Characterization of Structural and Mechanical Properties of Boron Nitride Nanotubes in High Temperature Environments. *Sci. Rep.* **2017**, *7*, 1–9. [CrossRef]
46. Al-Gaashani, R.; Radiman, S.; Daud, A.; Tabet, N.; Al-Douri, Y. XPS and optical studies of different morphologies of ZnO nanostructures prepared by microwave methods. *Ceram. Int.* **2013**, *39*, 2283–2292. [CrossRef]
47. Luo, T.; Chen, X.; Wang, L.; Wang, P.; Li, C.; Zeng, H.; Cao, B. Green laser irradiation-stimulated fullerene-like MoS_2 nanospheres for tribological applications. *Tribol. Int.* **2018**, *122*, 119–124. [CrossRef]
48. Zhao, B.; Yu, X.; Liu, Y.; Yang, L.; Zhang, Z.; Zhang, B. Frictional characteristics of heterostructure film composed of graphene and H-BN with the consideration of defects. *Tribol. Int.* **2021**, *153*, 106607. [CrossRef]
49. Garcia, M.A.L.; Martinez, A.I.; Castro, M.R.; Falcony, C.; Escobar, L.A. Correlation between structural and magnetic properties of sprayed iron oxide thin films. *Phys. B.* **2011**, *406*, 1496–1500. [CrossRef]
50. Li, W.; Luo, T.; Zhu, C.; Zhang, B.; Cao, B. Graphene/h-BN Nanosheet/Nanosphere Composites Constructed by In Situ Laser Irradiation with Synergistically Improved Tribological Performance. *Ind. Eng. Chem. Res.* **2023**, *62*, 435–444. [CrossRef]